MODELING OF THE FLAME ACCELERATION IN FLAT LAYER FOR HYDROGEN-AIR MIXTURES

J. Yanez, A. Kotchourko, M. Kuznetsov, A. Lelyakin, T. Jordan
Karlsruhe Institute of Technology, PO Box 3640, 76021 Karlsruhe, Germany,
alexei.kotchourko@kit.edu

ABSTRACT

The flame propagation regimes for the stoichiometric hydrogen-air mixtures in an obstructed semi-confined flat layer have been numerically investigated in this paper. Conditions defining *fast* or sonic propagation regime were established as a function of the main dimensions characterizing the system and the layout of the obstacles. It was found that the major dependencies were the following: the thickness of the layer of H_2-air mixture, the blockage ratio, and the distance between obstacles and the obstacle size. A parametric study was performed to determine the combination of the above variables prone to produce *strong* combustions. Finally, a criterion that separates experiments resulting in *slow* subsonic from *fast* sonic propagations regimes was proposed.

NOMENCLATURE

Latin			L	Integral scale of the turbulence	m
A	Constant in eq. (1)	-	l	Vertical interval between obstacles	m
b	Explanatory variable	-	l_0	Distance to first obstacle from the top	m
B R	Blockage ratio	-	n	Exponent in decay law of turbulence	-
C	Shape dependent constant, eq. (6)	-	S_t	Turbulent flame velocity	m/s
c_u	Sound speed in the reactants	m/s	S_u	Laminar flame velocity	m/s
c_p	Sound speed in the products	m/s	u'	Turbulence intensity	m/s
D	Horizontal interval between obstacles	M	u_0	Fluid velocity at the gaps between obstacles in the last reached vertical set	m/s
f	Gap at the top factor, eq. (8)	-	x_0	Horizontal position of previous obstacle	m
H	Thickness of the hydrogen layer	M	Greek		
h	Vertical dimension of the obstacle	M	ε	Turbulent dissipation	m^2/s^3
k	Turbulent kinetic energy	m^2/s^2	χ	Thermal conductivity	m^2/s

1.0. INTRODUCTION

Premixed combustions which are the object of the current work typically initiated by a weak source of energy, like a spark, which triggers the ignition of the reactive mixture. The flame begins to propagate slowly with a velocity which depends on the mixture reactivity and varies between several centimeters and several meters per second. At the same time due to existence of the obstacles and of the confinement, the flame can undergo strong acceleration and reach velocities up to hundreds meters per second. The expansion of the burned gases generates turbulence that through a feedback mechanism increases the effective burning rate causing a faster expansion. Such feedback results in flame acceleration with high pressure waves and, under certain circumstances, transition to a detonation. This positive feedback loop can be weakened, or even interrupted, by the tendency of the flame to quench due to flame stretch and heat losses. Additionally, venting would cause energy and momentum losses that can slow down the flame and prevent detonations and sonic propagation regimes.

Many of the topical studies dedicated to the acceleration of flames were performed in obstructed channels and have devoted a special emphasis to the deflagration to detonation transition (DDT), e.g., [1, 2]. In [3 - 5] the criteria able to predict the flame propagation regime for experiments in the tubular configurations were developed. In accordance with them, the expected regimes should depend on the tube geometry, and specifically, on the configuration of the obstacles. Then, the propagation regime can be categorized as *slow* sub-sonic, *fast* sonic (choked) and *quasi-detonations* (due to the significant pressure losses in the baffles the Chapman-Jouguet propagation velocity is not reached in the obstructed tubes).

Fast and quasi-detonations explosions can be suppressed in case of venting. In [6, 7] the effect of the lateral venting on flame acceleration and DDT was experimentally studied. It was found that the energy of reactive mixture necessary for the development of sonic flames or DDT grows with an enlargement of the venting surface. A comparative examination of the end- and side-vented explosions in tubes was carried out in [8].

Recently, explosions in obstructed semi-confined flat layer filled with uniform hydrogen-air mixtures have been examined. Such configuration mimics the release of H_2 into a room or a partially closed chamber and is important for many practical situations. In [15, 16] the effects of mixture reactivity and of the thickness of the flat layer of H_2-air mixture on the flame propagation regimes were analyzed. Critical conditions for sonic flame propagation and detonation onset were formulated.

In this paper the identical configuration of semi-confined flat layer was numerically examined. The main goal of the current work was, on the basis of the parametric study, to refine the requirements to geometrical configurations necessary to induce *fast* flame propagation regime. As a result of the numerical experiments, a criterion accounting the geometrical configuration of the facility and obstacles required for flame acceleration was elaborated.

2.0. DESCRIPTION OF THE EXPERIMENTAL FACILITY

The experimental work on hydrogen combustions in semi-confined layers [15, 16] was carried out inside the safety vessel named A1, see Figure 1 left. A rectangular box with dimensions of 9 x 3 x 0.6 m (Figure 1 right) was installed inside the protective container. The box itself involves a set of external metal frames, lined with smooth composite alumina-plastic plates on the interior side. The ratio of the volume of the reactive mixture volume to the total one of the safety vessel was equal to 0.16. The distance from the underside of the box to the floor was a minimum of 1.7 m. The conditions for a semi-confined combustion of a flat layer of reactive gases were assured by the disposition of the set up.

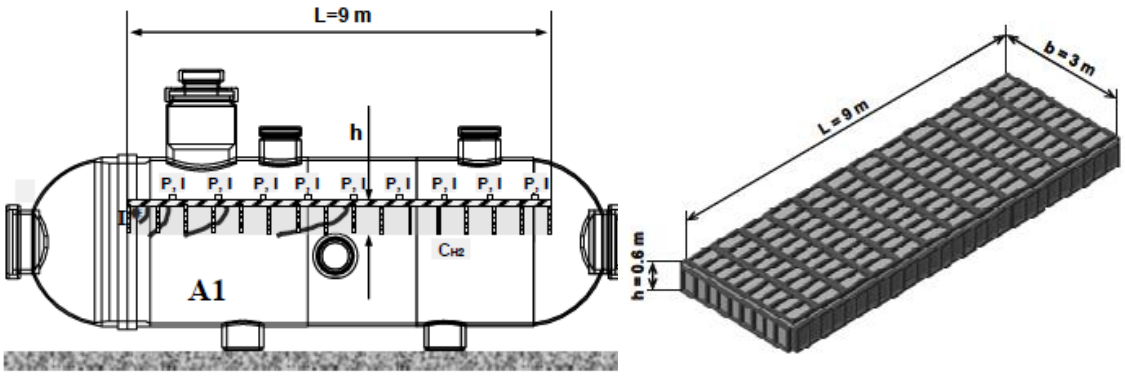

Figure 1 Experimental set up. Left, protective vessel with the box located in the interior. Evolution of the flame sketched in the interior. Right, arrangement of the flat layer box with metal frames.

The performed numerical simulations utilized a simplified schema of the facility (Figure 2). Since the existence of the protective vessel should not significantly affect the simulation results, the protective vessel was disregarded. Only the flat layer and the layout of the obstacles were modelled. Such a reduced outline was considered as sufficient to perform a parametric analysis of the geometrical configurations which induce *fast* flames for a single composition mixture. Contrary to the experimental studies, in which hydrogen concentration was varied in the range of 13-28 vol.%, the current work was focused on the influence of the geometrical parameters only.

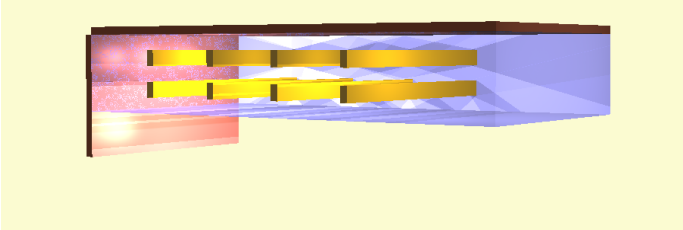

Figure 2. Simplified schema of the flat layer box considered in numerical experiments. Marked in yellow, a set of obstacles inside the flat H_2 layer.

3.0. SIMULATIONS

3.1. Numerical code

Numerical simulations were carried out with the combustion code COM3D [9] developed in the Karlsruhe Institute of Technology. The main characteristics of the code are summarized in the Table1.

Table 1: COM3D characteristics.

Type of solver	Discretization scheme	Time step requirement	CPU type, RAM and CPU time
Finite differences Fully compressible scheme	C^* = TVD 2^{nd} order D^* = 2^{nd} order central differences T^* = 2^{nd} order explicit	CFL = 0.94	32 processors Opteron-AMD 1 GB RAM per processor CPU time: ~24 hours

*C - convection terms; D - diffusion terms; T – time stepping

3.2. Numerical mesh and models

The different meshes representing the geometry of the experimental facility were created for each of the particular configuration of the obstacles. Two dimensional simulations were performed to maintain reasonable performance with high enough resolution. This restriction did not noticeably limit the capability of the simulations to capture all the significant physical phenomena. Comparison of the simulations and two dimensional vertical patterns from the experiments show that the deviations are not substantial. Open non-reflective boundary conditions were utilized to reproduce the release of the combustion products outside the hydrogen layer.

Table 2: Main characteristics of the numerical mesh used in the calculations**.**

Type of grid	Domain size, cells	Control cells	Cell size, m
Cartesian structured	400 × 1800	720,000	0.005

The most significant details of the mesh utilized in the calculation are enclosed in Table 2.The simulation of turbulence was carried out with the standard k-ε model [10]. The use of *Large Eddy Simulation* methods for the turbulence modeling [11] was not considered due to utilization of a two dimensional grid. The initial levels of turbulence intensity and dissipation were selected following the

criteria of Arntzen [12]. The combustion was modeled utilizing the KYLCOM model [13] coupled with the turbulent burning velocity correlation proposed by Schmidt [14].

3.3. Parametric study

Numerical experimental matrix (Table 3) was shaped out taking into account the main possibly significant geometrical parameters of the layout: the interval between obstacles, the thickness of the hydrogen layer, as well as the variables describing the blockage ratio, namely, the vertical interval between obstacles, and the height of the obstacles (Figure 3). As an additional parameter, the distance from the first obstacle to the top was also considered.

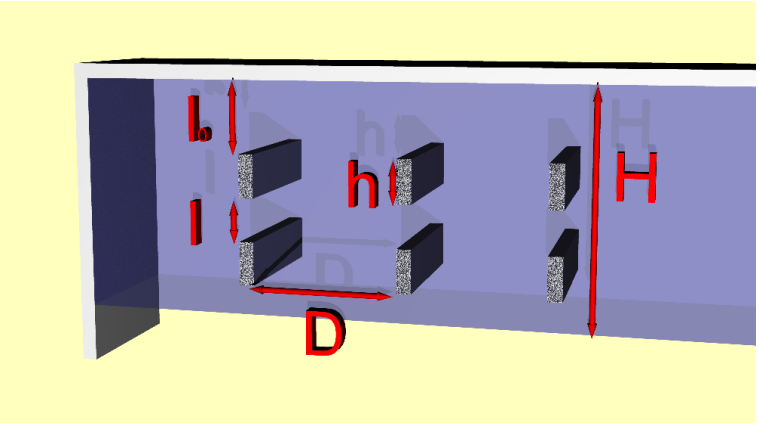

Figure 3. Main geometrical variables of the parametric study matrix.

4.0. RESULTS AND DISCUSSION

4.1. Qualitative analysis

After the ignition of the gaseous mixture (ignition point, top left corner, Figure 4), the flame initially propagates in a *quasi-laminar* regime. The visible flame velocity mainly depends on the intensity of the ignition source. Up to the first obstacle (top left picture, Figure 4) the flame front is very similar to a horizontal cylindrical surface.

Thereafter, depending on the geometrical configuration two scenarios were realized. The flame can accelerate to sonic speed, due to the turbulence generated by the obstacles (top right and bottom pictures, Figure 4). Alternatively, it can continue to propagate with subsonic velocity. In this last case, the energy and momentum losses through the vent area dominate over the *piston effect* from the flame itself.

Table 3. Main geometrical parameters of the matrix of numerical experiments.

Case	*D*, [m]	*H*, [m]	*BR*	*h*, [m]	l_0, [m]	*l*, [m]
4	0,60	0,60	0,50	0,06	0,06	0,06
5	0,60	0,20	0,50	0,06	0,06	0,06
6	0,60	0,30	0,50	0,06	0,06	0,06
7	0,60	0,15	0,50	0,06	0,06	0,06
8	0,30	0,20	0,50	0,06	0,06	0,06
9	0,30	0,15	0,50	0,06	0,06	0,06
14	0,30	0,30	0,50	0,06	0,06	0,06
15	0,15	0,30	0,50	0,06	0,06	0,06
16	0,15	0,10	0,50	0,06	0,06	0,06
17	0,15	0,10	0,50	0,06	0,06	0,06
18	0,90	0,30	0,50	0,06	0,06	0,06

19	0,90	0,20	0,50	0,06	0,06	0,06
20	0,90	0,15	0,50	0,06	0,06	0,06
21	0,90	0,10	0,50	0,06	0,06	0,06
22	0,60	0,30	0,30	0,04	0,08	0,08
23	0,60	0,20	0,30	0,04	0,08	0,08
24	0,60	0,15	0,30	0,04	0,08	0,08
25	0,60	0,30	0,70	0,09	0,04	0,04
26	0,60	0,20	0,70	0,09	0,04	0,04
27	0,60	0,15	0,70	0,09	0,04	0,04
28	0,60	0,30	0,90	0,11	0,01	0,01
29	0,60	0,20	0,90	0,11	0,01	0,01
30	0,60	0,15	0,90	0,11	0,01	0,01
31	0,60	0,30	0,50	0,10	0,11	0,11
32	0,60	0,20	0,50	0,10	0,11	0,11
33	0,60	0,15	0,50	0,10	0,11	0,11
34	0,60	0,30	0,50	0,30	0,30	0,30
35	0,60	0,30	0,50	0,15	0,15	0,15
36	0,60	0,20	0,50	0,30	0,30	0,30
37	0,60	0,30	0,70	0,09	0,00	0,04
38	0,30	0,15	0,50	0,06	0,00	0,06
39	0,60	0,30	0,90	0,11	0,00	0,01

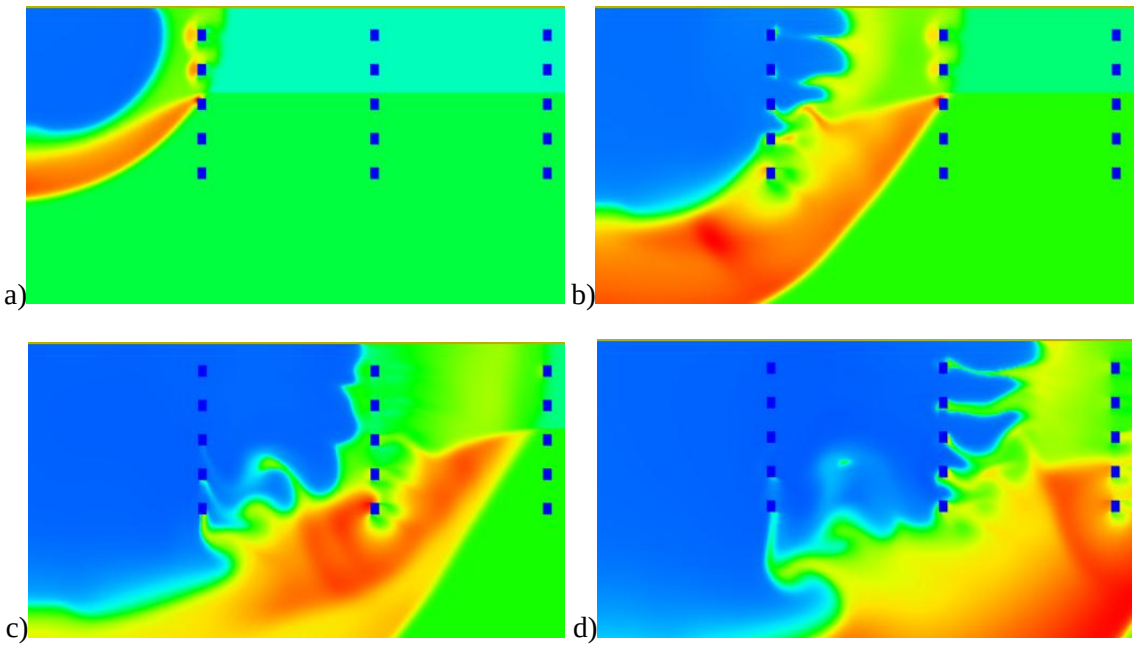

Figure 4. Density field for case 22 for a) 0.001, b) 0.002, c) 0.003, and d) 0.004 s after ignition.

4.2. Propagation regimes

These two possible scenarios are clearly visible in the Figure 5. The cases 15 and 26 represent *fast* sonic flames while the case 24 corresponds to a *slow* propagation. After the ignition, high velocities of around 600 m/s are achieved due to the expansion of the ignition charge. Around 40 cm apart from the ignition location different patterns start to be visible in the figure.

To objectively distinguish *fast* and *slow* combustion regime a physically pronounced criterion should be chosen. Table 4 offers a résumé of the results obtained in the numerical experiments. Additionally, a comparison of the velocities with the sound speed both in products and in reactants is included. To

exclude the effects of the expansion of the source used to simulate the ignition, the first 4 m of the facility were not considered. With the purpose of improving the performance of the calculations, for problems delivering *very slow* propagation regimes, the authors have not calculated the whole propagation of the flame. These cases are marked with the symbol '-'.

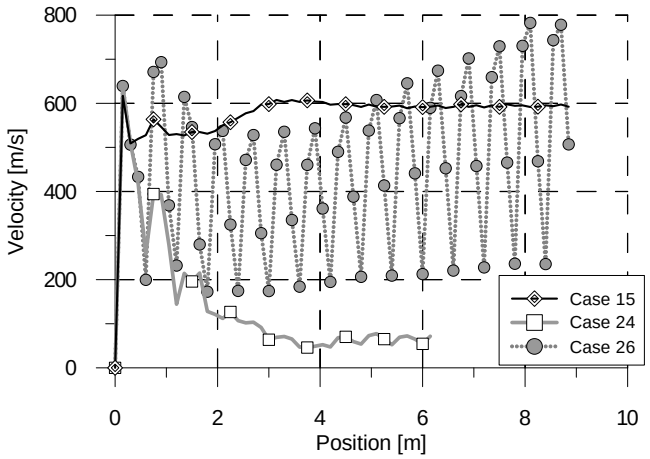

Figure 5. Registered flame velocities. Case 15, *fast* flame with small interval between obstacles, propagation velocity almost constant; Case 24, *fast* flame with increased interval between obstacles, high variance of the velocity; Case 26, decaying *slow* flame. Geometrical characteristic of every of those calculation cases can be found in Table 3.

Two criteria defining if the flame is *fast* were considered: first, if $E(v) > C_u$, and, second, if $v_{max} > C_u$. Results of the both criteria were almost coincident. Since the DDT process was not considered, the fastest propagation regime achievable in the simulations was the *choked* combustion. In this regime the obstacles work as a *bottle neck* limiting the speed of the gases through them. In the fastest problem analyzed, the maximum speed $v_{max} \approx 0.8\, C_p$ was found (Table 4).

4.3. Grid similarity analysis

The configuration of the system, with multiple obstacles and orifices, gives a hope that an analytical dependencies can be obtained considering the obstacles to be similar to a grid. Turbulence generated by a grid has been widely studied, i.e. [12]. In such configuration, the turbulent kinetic energy and the dissipation of turbulence decay as power laws

$$k = u_0^2 A \left(\frac{x - x_0}{l} \right)^{-n} \Rightarrow u' = \sqrt{\frac{2}{3}} A u_0 \left(\frac{x - x_0}{l} \right)^{-\frac{n}{2}}, \quad \text{and} \quad \varepsilon = \frac{An}{l} u_0^3 \left(\frac{x - x_0}{l} \right)^{-(n+1)}. \tag{1}$$

Substituting in the expression for L,

$$L = \frac{\sqrt{Al}}{n} \left(\frac{u'}{\sqrt{A} u_0} \right)^{\frac{n-2}{n}} \Rightarrow L = \frac{\sqrt{Al}}{n} \left(\frac{x - x_0}{l} \right)^{\frac{-n+2}{2}}. \tag{2}$$

For the previous laws, it was found experimentally that $n = 1.3$. Taking into account that the Schmidt correlation reads as

$$S_t = S_u + u' \sqrt{1 + \left(\frac{u' \chi}{L S_u^2} \right)^2}, \text{ and then, } \quad S_t \sim u'^{\frac{n+2}{n}} \approx u'^{2.46}. \tag{3}$$

Additionally,

$$S_t \sim \left(x - x_0\right)^{-\frac{n+2}{2}} \approx \left(x - x_0\right)^{-1.65} \text{. and the same reasoning delivers } S_t \sim u_o^{\frac{3n-2}{n}} \approx u_0^{1.46}. \quad (4)$$

Table 4. Results obtained in the numerical experiments. Values obtained excluding the first 4 m of the facility. Average speed *E(v)*, maximum speed v_{max}, standard deviation of the speed *Var(v)*, Mach numbers obtained from the average speed related to the sound speed in the reactants $E(v)/C_u$, to the products $E(v)/C_p$; from the maximum speed to the sound speed in the products v_{max}/C_p; and minimum speed to the sound speed in the reactants v_{min}/C_u. *Fast* propagation regime are marked with *'#'*.

Case	*E(v)*	v_{max}	v_{min}	$\sigma(v)$	$E(v)/C_u$	$E(v)/C_p$	v_{max}/C_p	v_{min}/C_u	$E(v)>C$	$v_{max}>C_u$
4	640,4	899,3	303,8	193,1	1,56	0,80	0,88	0,74	#	#
5	-	-	-	-	-	-	-	-		
6	549,2	766,0	310,6	151,2	1,34	0,68	0,75	0,76	#	#
7	266,2	360,3	177,9	58,6	0,65	0,32	0,35	0,43		
8	508,1	682,5	334,7	132,8	1,24	0,61	0,67	0,82	#	#
9	483,7	658,2	322,5	123,2	1,18	0,59	0,65	0,79	#	#
14	589,4	748,0	439,9	108,5	1,44	0,67	0,73	1,07	#	#
15	594,2	603,1	588,7	3,0	1,45	0,54	0,59	1,44	#	#
16	296,8	407,5	247,4	48,8	0,72	0,36	0,40	0,60		
17	-	-	-	-	-	-	-	-		
18	189,3	288,2	93,6	51,2	0,46	0,26	0,28	0,23		
19	86,4	147,0	45,4	30,9	0,21	0,13	0,14	0,11		
20	-	-	-	-	-	-	-	-		
21	-	-	-	-	-	-	-	-		
22	275,3	361,3	200,9	40,2	0,67	0,32	0,35	0,49		
23	81,3	105,5	61,9	12,2	0,20	0,09	0,10	0,15		
24	63,5	77,6	47,4	9,1	0,16	0,07	0,08	0,12		
25	531,4	806,3	220,9	210,0	1,30	0,72	0,79	0,54	#	#
26	488,4	782,4	194,9	188,0	1,19	0,70	0,77	0,48	#	#
27	360,1	548,2	168,7	99,5	0,88	0,49	0,54	0,41		#
28	501,1	737,7	134,3	196,5	1,22	0,66	0,72	0,33	#	#
29	445,5	667,3	127,7	169,9	1,09	0,60	0,65	0,31	#	#
30	-	-	-	-	-	-	-	-		
31	544,2	799,6	265,3	183,8	1,33	0,71	0,78	0,65	#	#
32	120,2	179,2	83,5	30,8	0,29	0,16	0,18	0,20		
33	-	-	-	-	-	-	-	-		
34	112,3	150,5	58,2	31,2	0,27	0,13	0,15	0,14		
35	184,3	282,2	108,3	43,7	0,45	0,25	0,28	0,26		
36	-	-	-	-	-	-	-	-		
37	-	-	-	-	-	-	-	-		
38	479,2	482,2	475,9	1,8	1,17	0,43	0,47	1,16	#	#
39	-	-	-	-	-	-	-	-		

For the space dependence

$$S_t \sim l^{\frac{n}{2}} \approx l^{0.65}. \quad (5)$$

Roach [12] utilizes an alternative formulation in function of the size of the obstacle *h*. Under his approach,

$$u' = UC\left(\frac{x - x_0}{h}\right)^{-\frac{5}{7}}, \text{ and } \quad L = 0.2h\left(\frac{x - x_0}{h}\right)^{\frac{1}{2}}. \tag{6}$$

This means that,

$$S_t \sim \left(x - x_0\right)^{-1.6}, \quad \text{and} \quad S_t \sim h^{0.92}. \tag{7}$$

4.4. Analysis of the standard deviation of the propagation velocity

The variance or standard deviation of the propagation velocity is the main characteristic of the *fast* propagation regimes. The rationale contained in previous sections suggests, based on the formulation appearing in [12] to try to describe the dimensionless standard deviation $\sigma(v)/E(v)$ as a function of the explanatory variable $B=D^{1.65}l^{-0.65}$. Alternatively, a correlation of the standard deviation can be obtained by means of the Roach's formulation utilizing the explanatory variable $B=D^{1.6}h^{-0.9}$. In Figure 6, the correlations obtained by the use of both approaches are represented. In both cases, the approximation was improved taking the square root of the variable *B*, so that finally, the variable considered in abscissas was $B'=(D^{1.65}l^{-0.65})^{1/2}$ and $B'=(D^{1.6}h^{-0.9})^{1/2}$. Both approximations deliver a correlation coefficient of 0.53 and 0.44 for Pope and Roach formulations respectively. This means that the divergences, characterized by a moderate correlation coefficient, are very important.

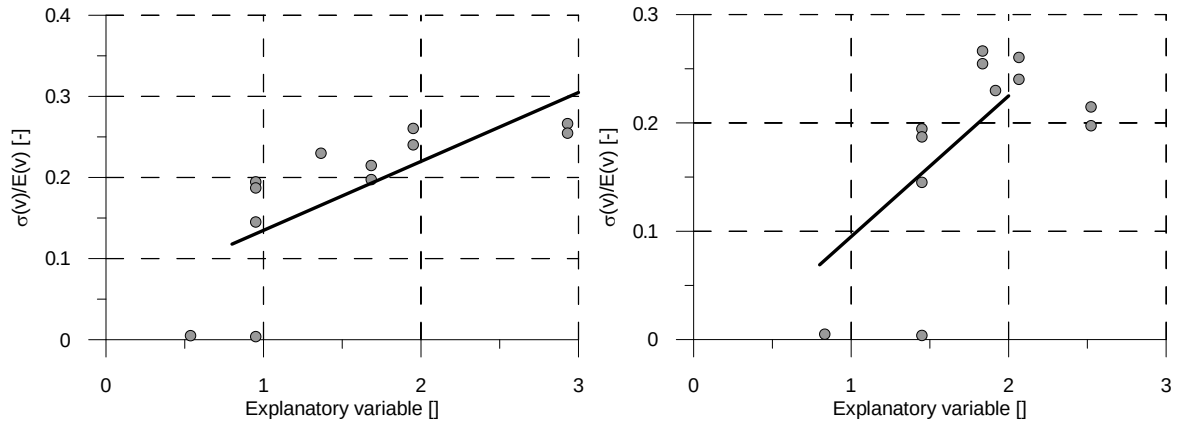

Figure 6. Dimensionless variance vs explanatory variable. In black, tendency line. Left, based in Pope method, considering $B = \sqrt{D^{1.65} l^{-0.65}}$ as explanatory variable with correlation coefficient 0,53. Right, based in Roach's approach, with explanatory variable $B = \sqrt{D^{1.6} h^{-0.9}}$ correlation coefficient 0.44.

The correlation coefficient increases if further square roots of the explanatory variable are considered (see Figure 7). This suggests a complex dependence on the combination of the selected variables which reads as $Var(v)/E(v) \approx \sum_i a_i (D^{1.65} l^{-0.65})^{1/i}$.

For geometries which strongly differ from grid pattern, such as for the cases in which there exists a high blockage ratio, superior results may be derived considering other forms of self-similar flows, as the planar jet.

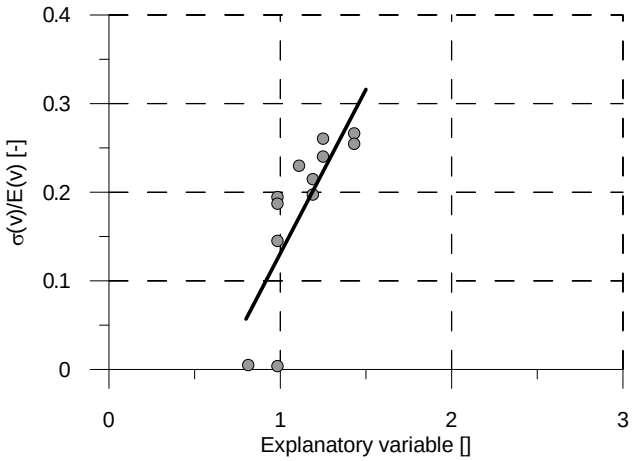

Figure 7. Dimensionless variance vs. explanatory variable. In black, tendency line. Explanatory variable based in Pope method considering $B = \sqrt[6]{D^{1.65} l^{-0.65}}$ with correlation coefficient 0,66.

4.5. Effect of blockage ratio and importance of top gap l_0

The blockage ratio has an additional significant effect that must be considered in the current analysis. The propagation of the flame through the set of vertical obstacles can have two different modes. In the case of *low* blockage ratio equal to 0.3 (Figure 8, left), the flame front advances so that the flame traverse the three upper orifices almost simultaneously; in the case with blockage ratio 0.9 (Figure 8, right), the flame traverse the vertical set of obstacles only through the upper gap. In this last case, the whole process is as follows. After the flame has entered in the *cubicle* (space between two set of vertical obstacles) the propagation continues with a decreasing velocity. The products of the combustion accumulate at the top of the facility. The expansion of the products creates a motion which is partially discharged through the gaps between obstacles. When a sufficient amount of products are accumulated all over the place, the expansion of the products creates a flow through the gaps which is intense and highly turbulent. At the moment when the flame goes through the obstacles the combustion rate suffers an intense acceleration due to the interaction with the turbulence. The combination of the intense flow through the gap and the flame turbulence interaction produces the spurt of the flame through the upper hole into the next *cubicle*.

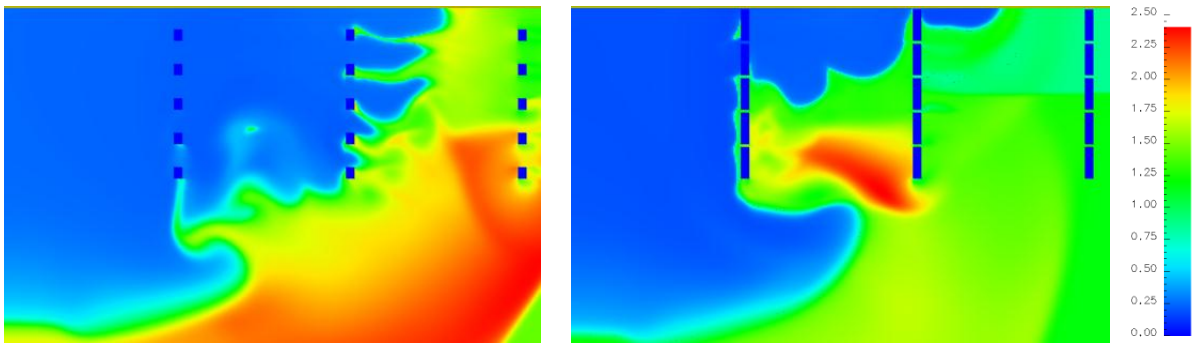

Figure 8. Left, Case 22 (left) and Case 28 (right) 0.004 s after ignition.

This qualitative behavior gives an indication that for the systems with higher blockage ratios the existence or not of an opening at the top, between the horizontal ceiling and the first obstacle, can be decisive. This statement was confirmed by the results of the simulations. *Fast* propagation regime was obtained in the tests number 9, 25 and 28. These cases were repeated using the same layout for the obstacles excluding the gap at the top, the tests 37-39. The results obtained show that the fast

propagation was only achieved for the configuration with relatively low blockage ratio (*BR*=0.5) case 38.

The absence of the aperture at the top can severely restrict the propagation of the flame. The reason of it can be clearly understood. After the flame penetrates in the *cubicle* an accumulation of products in the closed top of the facility is created. The flow of gases cannot be, even partially, discharged horizontally. The products expand downwards and eventually traverse the almost closed baffle through the first and/or the second gap.

4.6. Acceleration criteria

A criterion, defining whether the propagation regime found in the numerical experiment will be *fast*, can be obtained on the basis of the results presented in the previous sections. Such criteria can provide useful information for the experimentalists and for the practical applications, as in [3 - 5].

One of the important conclusions made in the course of the analysis of the observations, consists in the following: the blockage ratio cannot be used independently as an explanatory parameter of the mixture behavior. The confirmation of this fact follows from the diagram presented in the Figure 9. Nevertheless, the figure also reveals that the criteria for the separation of fast and slow numerical experiments must contain the blockage ratio as one of the variables involved in the final formula. It follows, e.g., from the fact that no experiments with low blockage ratio $BR \approx 0.3$ reached high propagation velocities.

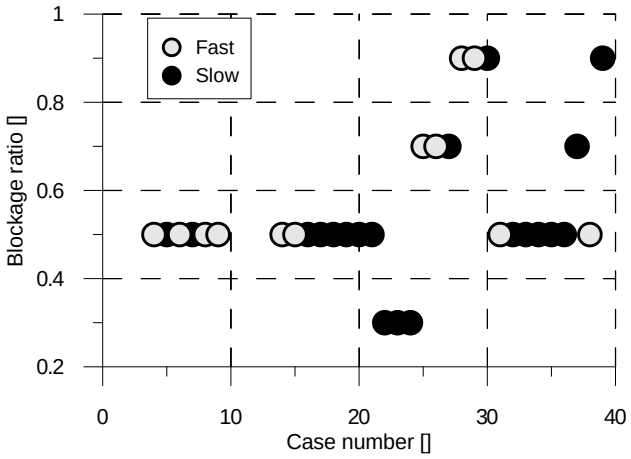

Figure 9. Blockage ratio as a single explanatory parameter for the results obtained in the different calculations.

The total energy contained in the system is proportional to *H*. The flame velocity may be considered inversely proportional to *D*. This can be inferred seeing eq. (6) and the dependence on the standard deviation. At the same time, and for the same reasons, it is proportional to *h*. Therefore, the dimensionless variable *D/h* can be utilized to characterize the system. Also, the blockage ratio is an important factor characterizing the problems. For the cases, in which the blockage ratio is high, the dependence on l_0 looks to be also significant. The l_0 variable could be naturally made dimensionless by means of *l*. The parameter *H* can be normalized using *l* or *h* variables. The trial and error approach provides better separation for *h* variable. Thus, the set of variables *H/h*, l_0/l, *D/h*, *BR* can be combined to obtain a criteria for the development of fast and slow flames. After a thorough investigation the variable

$$B = \frac{H}{h} BR \cdot f; \quad f = \begin{Bmatrix} l_0 / l; & BR \geq 0.7 \\ 1; & BR \leq 0.7 \end{Bmatrix}, \tag{8}$$

was chosen to create a separation criterion. The result achieved is illustrated by the Figure 10. A very good separation between the cases in which the flame propagation regime was fast and slow was attained.

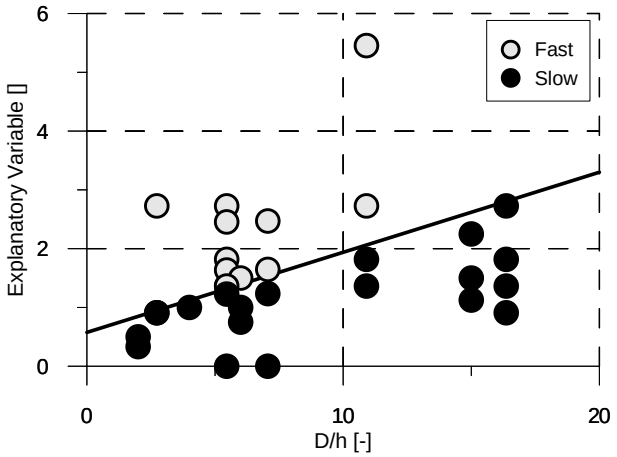

Figure 10. Application of the criterion (9) for all performed numerical experiments. Fast flames are depicted by the grey points, the slow flames are depicted by the black points.

The line separating fast and slow flames in the diagram in the Figure 10 and, consequently, the corresponding criteria for flame acceleration reads as

$$\frac{H}{h} BR \cdot f > 0.136 \frac{D}{h} + 0.575 . \tag{9}$$

Assuming $l = l_0$ and dividing by $H/h \cdot BR \cdot f$ and multiplying by expansion ratio of test mixture $\sigma^*=7.0$ one can transform criteria to the criteria for critical expansion ratio

$$\sigma > \sigma^* \left(0.575 \frac{h}{H} \frac{1}{BR} + 0.136 \frac{D}{H \cdot BR} \right). \tag{10}$$

Substituting $BR = n \cdot h/n/(h+l) = n \cdot h/H$ and $\sigma^* = 1.87 \cdot \sigma_0^*$, where n is the number of beams; $\sigma_0^* = 3.75$ is the critical expansion ratio for hydrogen-air mixtures at normal conditions [4], the criteria (9) can be shaped in the form used in [15]

$$\sigma > \sigma_0^* \left(\frac{1}{n} + 0.25 \frac{1}{BR} \frac{D}{H} \right). \tag{11}$$

Note, that the equation (11) at $n = 1$ and $BR = 0.5$ looks qualitatively similar to that obtained in [15] which is based on the experimental data analysis. The only difference is that quantitatively the slope of the dependency against the parameter D/H is three times less than in the experiments. On the other hand in comparison with [15], the criterion (11) provides noticeably higher level of the generality due to additional accounting of the effect of blockage ratio variation.

5.0. SUMMARY

This paper presents the first results of a large-scale numerical study on flame acceleration in obstructed semi-confined flat layers of uniform stoichiometric hydrogen-air mixtures. The effects of obstruction arrangement within the semi-confined layer, described by the distance between obstacles, the thickness of the hydrogen layer, the blockage ratio, the sizes of the obstacles and the orifices, on the flame propagation regime was analyzed. The set of the dimensionless parameters and the

dependence linking them (9), which permits credible separation of the fast and slow propagation regimes, were proposed. Additionally, it was shown that the standard deviation of the velocity, characterizing the effect of the obstacle structure on the flame behavior, can be characterized with the variable $(D^{1.65}l^{-0.65})$.

REFERENCES

1. Bradley, D., Lawes, M., Kexin Liu., Turbulent flame speeds in ducts and the deflagration/detonation transition. Combustion and flame, 154, 2008, pp. 96-108.
2. Oran, E.S.; Gamezo, V.N., Origins of the deflagration-to-detonation transition in gas-phase. Combustion and Flame, 148, vol. 1-2, 2007, pp. 4-47
3. Dorofeev, S.B., Sidorov, V.P., Kuznetsov, M.S., Matsukov, I.D., Alekseev, V.I., Effect of scale on the onset of detonations. Shock Waves, 10, 2000, pp. 137-149
4. Dorofeev, S.B., Kuznetsov, M.S., Alekseev, V.I., Efimenko, A.A., Breitung, W., Evaluation of limits for the effective flame acceleration in hydrogen mixtures. Journal of loss prevention in the process industries, 14, 2001, pp. 583-589.
5. Kuznetsov, M., Alekseev, V., Yankin, Y., Dorofeev, S., Slow and fast deflagration in hydrocarbon-air mixtures. Combustion Science and Technology, 174, 2002, 157-172
6. Ciccarelli, G., Boccio, J., Ginsberg, T., Finfrock, C., Gerlach, L., Tagava, H., & Malliakos, A., The effect of lateral venting on deflagration-to-detonation transition in hydrogen–air steam mixtures at various initial temperatures. NUREG/CR-6524, BNLNUREG-52518. Washington, DC: US NRC, 1998.
7. Alekseev, V. I., Kuznetsov, M. S., Yankin, Yu. G., Dorofeev, S. B. Experimental study of flame acceleration and the deflagration-to-detonation transition under conditions of transverse venting, Journal of Loss Prevention in the Process Industries, 14, 6, 2001, pp. 591-596.
8. Alexiou, A., Andrews, G.E., Phylaktou, H., A comparison between End-Vented and Side-Vented Gas Explosions in Large L/D Vessels, Process Safety and Environmental Protection, 75, 1, 1997, pp. 9-13.
9. Kotchourko, A., Breitung, W., Veser, A. Reactive Flow Simulations in Complex 3D Geometries Using The COM3D Code. 'Jahrestagung Kerntechnik' 99, Kerntechnische Gesellschaft e.V. Deutsches Atomforum e.V. Annual Meeting on Nuclear Technology, 1999
10. Launder, B. E., and Sharma, B. I. Application of the energy dissipation model of turbulence to the calculation of flow near near a spinning disk. Lett. Heat Mass Trans. 1, 1974, pp 131-137.
11. Jimenez, J. Turbulence and Vortex Dynamics. Notes for the Polytecnique course on turbulence. École Polytechnique, Paris, France, 2004 (privat communication).
12. Arntzen, Bjorn., Modelling of turbulence and combustion for simulation of gas explosions in complex geometries. Thesis for Dr. Ing Degree." The Norwegian university for science and technology. 1998.
13. Yanez, J., Kotchourko, A., Lelyakin, A., KYLCOM Model for the Calculation of Under-resolved Hydrogen Combustion Problems. Proceedings of the Sixth ISFEH. Leeds, 11st - 16th April, 2010 (in press).
14. Schmidt, H.P., Habisreuther, P., Leuckel, W., A Model for Calculation Heat Release in Premixed Turbulent Flames. Comb. Flame. 113, 1998, pp. 79-91.
15. Kuznetsov, M., Grune, J., Friedrich, A., Sempert, K., Breitung, W., Jordan, T., Hydrogen-Air deflagrations and Detonations in a semi-confined flat layer. Proc. Sixth International Seminar on Fire and Explosions Hazards. University of Leeds, Leeds, UK, paper 212, 2010, pp. 1-12.
16. Grune, J., Sempert, K., Haberstroh, H., Kuznetsov, M., Jordan, T., Experimental investigation of hydrogen-air deflagrations and detonations in semi-confined flat layers. 8th ISHPMIE September 5-10, 2010, Yokohama, Japan
17. Stephen B. Pope, Turbulent Flows, Cambridge University Press 2000
18. P. Roach, The generation of nearly isotropic turbulence by means of grids, J. Heat Fluid Flow 8, 1987, pp. 82–92